International Journal of Engineering & Technology
CENTRE OF PROFESSIONAL RESEARCH PUBLICATIONS
ISSN 2049-3444

International Journal of Engineering and Technology Volume 3 No. 4, April, 2013

An Effective Finite Element Method for Beam Based Compliant Mechanism

Theddeus T. Akano, Omotayo A. Fakinlede
Department of Systems Engineering, University of Lagos, Akoka, Lagos.

ABSTRACT

This paper presents a nonlinear analysis of compliant mechanisms (CMs[i]) using finite element method. The case of a compliant four-bar mechanism, where the coupler link is to be guided by flexible input and follower links is developed. Previous works on this type of compliant mechanism are based on linear formulation thereby neglecting the shear stress induced in the links. An investigation on the influence of geometric nonlinearity in the analysis of compliant mechanisms where all flexible links are considered as two dimensional beams with shear deformation is presented. The energy equations were developed first; the discretization and the lagrangian dynamics that produced the motion equation were thereafter established. The automatic derivation of formulae needed in numerical procedure were done using symbolic programming module, AceGEN and implemented in a compiled back end, AceFEM. Finally, the numerical results reveal the deviation that exists with linear formulation assumption, showing that this approach is more encompassing.

Keywords: *Compliant Mechanisms, Symbolic Programming, Finite Element Method, AceGEN, AceFEM, Geometric Nonlinearity (GNL[ii])*

1. INTRODUCTION

A mechanism is a mechanical device which transfers forces and motions from an input source to output link [1]. A compliant mechanism (CM) is a mechanism that gains some or all of its motion from the deformation of slender segments rather than from relative motion between rigid-body links connected by joints [2]. The popularity of compliant mechanisms is expected to grow since the compliance grants the designer greater freedom in the number of possible solutions for a given problem. However, this freedom in design is often offset by difficulties encountered in the analysis of the compliant members. The use of compliance presents several advantages including part count reduction, absence of coulomb friction, no need for lubrication, more precise motion, compactness, etc. Recently, there are several examples of compliant mechanisms that have been designed and widely used in various fields such as for adaptive structures, biomedical, hand-held tools, components in transportations, Microelectromechanical Systems (MEMS[iii]) and robotics. However, the design of CMs is complicated by the flexible members which include elastic links and elastic hinges. These usually undergo large deflections which introduce geometric nonlinearities. Therefore, the study of large deflections in elastic beams has long been one of the central themes of interest aiming at accurately describing the deformation in CMs [2, 3]. Since in these applications, curvature is nonlinear due to geometrical nonlinearities, a nonlinear mathematical formulation should be considered. Consequently, deflections are difficult to determine by analytical methods, hence numerical method should be employed. Due to the complexity of the nonlinear governing equations, only a few studies have been carried out so far to investigate the nonlinear deformation of CMs [4-8].

A number of researchers have worked on the analysis of compliant mechanism using the Pseudo Rigid Body Model (PRBM[iv]) [9-16]. Some have also employed the application of finite element method on the analysis of compliant mechanisms [17-20]. Many other researchers have adopted many ways to synthesize the mechanism [21-32]. However, these analyses are based on linear assumptions. It is obvious that these cannot give a true understanding of the performance of compliant mechanisms. At present, there are few studies on the synthesis of compliant mechanisms by topology optimization based on large displacement of the mechanisms using geometrically nonlinear finite element models [33-36]. Geometric nonlinearity in the formulation of flexible multibody system dynamics may arise from an orientation change in the body through a number of rotations and from the occurrence of large displacements induced by elastic deformation. The former must always be considered in the analysis, even in dealing with systems consisting of bodies that are analysed under the rigid body hypothesis. However, the latter are only significant in those cases where strong deflections of the elements and/or major axial forces in the deformed configurations are considerably different from those for the undeformed configurations.

Previous works on this type of compliant mechanism neglected the shear stress induced in the links. The

pseudo-rigid body model neglects the shear stress and/or force that could be induced in the compliant links as they deflect, in order for a compliant mechanism to undergo any amount of motion. The pseudo rigid body model is replaced by a two-dimensional nonlinear finite element formulation for the beam with shear deformation.

We shall focus our work on a four-bar mechanism (See Fig. 1.), which is a closed-loop kinematic chain. One of the links is called the coupler link, and is the only one that can trace paths of arbitrary shape because it is not rotating about a fixed pivot. Apart from [37] which focused on the synthesis of the input and follower links simultaneously through optimisation of the finite element model, previous research on this type of mechanism comprised of at least one moving rigid link, and the coupler link was always considered a rigid member, because the motion generation objective is based on the task definition for conventional rigid-link mechanisms.

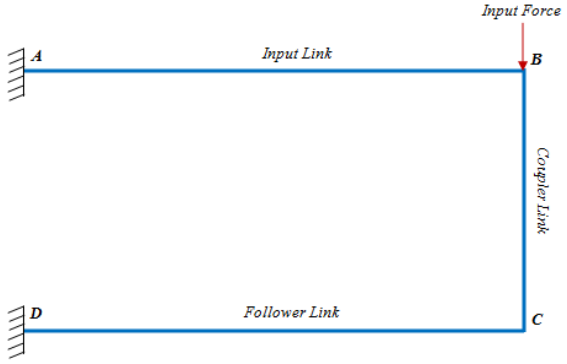

Fig. 1. A four-bar mechanism

In this paper, a compliant four-bar mechanism is considered, because all its motion is obtained from the deflection of compliant members. The bars are modeled as beams with shear deformation, thus involving the guidance of a flexible link rather than a rigid body.

This work uses a system of symbolic and algebraic programming (Mathematica) and within it a developed modules AceGen, AceFEM and AceShare [38] which together constitute a system named Symbolic Mechanics System [39]. Mathematica is a basic and very powerful tool for working with formulae and to perform various mathematical operations and expressions on computers. Modern versions include the possibility of presenting results and numerical analysis. AceGen is used for the automatic derivation of formulae needed in numerical procedures. The AceGen package also provides a collection of prearranged modules for the automatic creation of the interface between the automatically generated code and the numerical environment where the code would be executed. The AceGen package directly supports several numerical environments such as Mathlink, AceFEM, FEAP, FORTRAN, ELFEN and ABAQUS. AceFEM is a research finite element environment based on Mathematica, designed to solve multi-physics and multi-field problems. The AceFEM package explores the advantages of symbolic capabilities of Mathematica while maintaining numerical efficiency of commercial finite element environments.

The rest of the paper is organised as follows. Firstly, the energy equations were developed. Secondly, the motion equation was obtained. Finally, a numerical example of a compliant four-bar mechanism is given for the implementation of the model. The comparative analysis of the effect of geometric nonlinearity on the analysis of compliant mechanism is presented. Finally, a summary of the highlights of the work is given the conclusion section.

2. MATHEMATICAL MODEL

The model is based on the selection of the geometry, material properties, the loading and boundary conditions, and any other specific assumptions made. The purpose of the analysis is to answer certain questions regarding the stiffness, stresses developed and strength of the structure. Hence, when studying the behaviour of the structure, we would like to predict the future not only when the structure is operating in normal conditions, which mostly only requires a linear analysis, but also when the structure is subjected to severe loading conditions, which usually requires a highly nonlinear analysis.

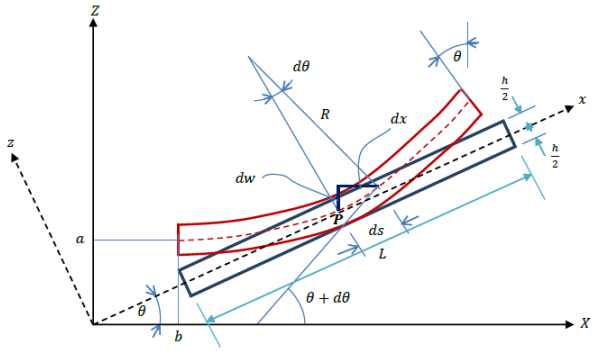

Fig. 2. Deformed and underformed beam element

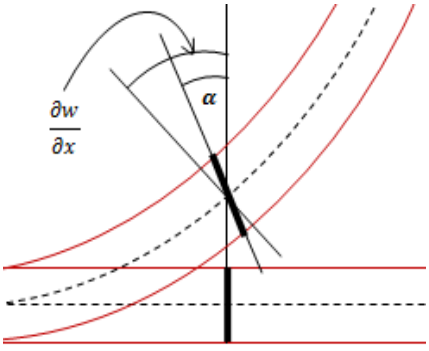

Fig. 3. Detail of the beam element with shear deformation

Figure 2 shows the deformed and underformed beam element in the x-z plane while Fig. 3. shows the detail of

the beam element with shear deformation. R is the radius of curvature of the beam. dx, dw and ds form a right angled triangle. ds is a very small portion on the centroid of the deformed beam element. L is the length of the beam element. The curvature k of the beam element is given as:

$$k = C\frac{d^2w}{dx^2} \tag{1}$$

Where

$$C = \frac{1}{\left(\sqrt{1+\left(dw/dx\right)^2}\right)^3} \tag{2}$$

Compliant members undergo large deflections which introduce geometric nonlinearity. For small deflection, the slope of the deflected middle surface are small compared to unity so that the curvature is approximated as:

$$k \approx \frac{d^2w}{dx^2} \tag{3}$$

The deviation of the value of C from unity represents the factor by which the compliant system undergoes large deflection.

2.1 Kinetic Energy

In Fig. 2. the displacement vector along the neutral axis in axial direction is given as

In Fig. 2. the displacement vector along the neutral axis in axial direction is given as

$$S_x = aCos\theta + bSin\theta + x + u \tag{4a}$$

$$S_z = bCos\theta - aSin\theta + w \tag{4b}$$

Eqs. (3) and (4) could be combined in the form

$$S = \left(aCos\theta + bSin\theta + x + u\right)i + \left(bCos\theta - aSin\theta + w\right)k \tag{5}$$

Where a and b are the coordinates of end 1 of the beam element. x is the coordinate measured along the element's neutral axis from 1 to 2. θ is the angle between the body motion and the x-axis. u and w are the axial and transverse displacements of point P from the rigid body position. For small value of θ, $Cos\theta \approx 1$ and $Sin\theta \approx \theta$. Substituting these values into Eq. (5), gives

$$S = \left(a + b\theta + x + u\right)i + \left(b - a\theta + w\right)k \tag{6}$$

Differentiating Eq. (6), the velocity of a particle at point, P is given as:

$$V = \frac{ds}{dt} = \left(b\frac{d\theta}{dt} + \frac{dx}{dt} + \frac{du}{dt}\right)i + \left(a\frac{d\theta}{dt} + \frac{dw}{dt}\right)k \tag{7}$$

The kinetic energy T_p of beam particles can be expressed as:

$$T_p = \frac{1}{2}\iint \rho\, A_x V^2 dxdz \tag{8}$$

Where ρ is the mass density of the beam material and A_x is the cross sectional area of the beam element. The kinetic energy T_s associated with transverse shear is also given as:

$$T_s = \frac{1}{2}\iint \rho\, I_z \left(\frac{d\alpha}{dt}\right)^2 dxdz \tag{9}$$

α is the measure of transverse shear angle. The angular velocity V_a of any differential line segment on the neutral axis of the element is given by

$$V_a = \frac{d\theta}{dt} + \frac{d^2w}{dxdt} \tag{10}$$

The kinetic energy T_R due to rotatory inertia of the beam element is given as

$$T_R = \frac{1}{2}\iint \rho I_z \left(\frac{d\theta}{dt} + \frac{d^2w}{dxdt}\right)^2 dxdz \tag{11}$$

The total kinetic energy T of the beam element becomes

$$T = T_p + T_s + T_R \tag{12}$$

It should be noted that the limits of the double integration in Eqs. (8), (9) and (11) are from $-h/2$ to $h/2$ and 0 to L. Eq. (12) becomes

$$T = \frac{1}{2}\left[\int_{-h/2}^{h/2}\int_0^L \left(\rho A_{xz}\left(\left(b\frac{d\theta}{dt} + \frac{dx}{dt} + \frac{du}{dt}\right)^2 + \left(a\frac{d\theta}{dt} + \frac{dw}{dt}\right)^2\right) + \rho\, I_z\left(\left(\frac{d\alpha}{dt}\right)^2 + \left(\frac{d\theta}{dt} + \frac{d^2w}{dxdt}\right)^2\right)\right)dxdz\right] \tag{13}$$

2.2 Strain – Displacement Relation

The Green strain u_x, u_y and u_z are displacements of the member at any point in the x, y and z directions respectively. u, v and w are displacements of the middle surface in the x, y and z directions respectively. The Green strain is given as

$$\varepsilon_{xx} = \frac{\partial u_x}{\partial x} + \frac{1}{2}\left[\left(\frac{\partial u_x}{\partial x}\right)^2 + \left(\frac{\partial u_y}{\partial x}\right)^2 + \left(\frac{\partial u_z}{\partial x}\right)^2\right] \quad (14)$$

The von Karman strains are related to the displacement by

$$\varepsilon_{xx} = \varepsilon_{xx}^0 + z\varepsilon_{xx}^1 \quad (15)$$

$$\varepsilon_{xx}^0 = \frac{\partial u_x}{\partial x} + \frac{1}{2}\left(\frac{\partial u_z}{\partial x}\right)^2 = \frac{\partial u_x}{\partial x} + \frac{1}{2}\left(\frac{\partial w}{\partial x}\right)^2 \quad (16)$$

$$\varepsilon_{xx}^1 = \frac{\partial^2 w}{\partial x^2} \quad (17)$$

Eq. (16) stands for the strain equation for geometric nonlinearity due to stretching of the neutral axis. Eq. (17) is equivalent to the curvature displacement relation for small deflection in Eq. (3). Therefore, for large deflection analysis which results in geometric nonlinearity due to curvature, Eq. (15) becomes

$$\varepsilon_{xx} = \varepsilon_{xx}^0 + zk \quad (18)$$

$$\varepsilon_{xx} = \frac{\partial u_x}{\partial x} + \frac{1}{2}\left(\frac{\partial w}{\partial x}\right)^2 + zC\frac{\partial^2 w}{\partial x^2} \quad (19)$$

In order to present realistic proportional links, the links are assumed to be of the same cross section. Each link is divided into elements of the same length with constant areas. The integrations involved in the element equations are carried out in a piecewise fashion with areas in each section taken as a constant.

2.3 Strain Energy

The virtual strain energy Ψ for the element may be written as

$$\Psi = \iint \sigma\delta\varepsilon \; dxdz + \frac{1}{2}\iint \tau_{xz}\gamma_{xz}\, dxdz \quad (20)$$

Where σ is the normal stress, ε is the normal strain, τ_{xz} and γ_{xz} are the shear stress and shear strain respectively.

But,

$$\tau_{xz} = G_{xz}\gamma_{xz} \;\; ; \;\; \gamma_{xz} = \left(\alpha + \frac{\partial w}{\partial x}\right)^2 \quad (21)$$

Where G_{xz} is the shear modulus. Substituting Eq. (21) into Eq. (20), we have

$$\Psi = \iint \sigma\delta\varepsilon \; dxdz + \frac{1}{2}\iint G_{xz}\left(\alpha + \frac{\partial w}{\partial x}\right)^2 dxdz \quad (22)$$

Differentiating Eq. (19), we have

$$\partial\varepsilon_{xx} = \frac{d\delta u}{dx} + \frac{\partial w}{\partial x}\frac{d\delta w}{dx} + zC\frac{\partial^2 \delta w}{\partial x^2} \quad (23)$$

Substituting Eq. (23) into Eq. (22) gives

$$\Psi = \iint \sigma_{xx}\left(\frac{d\delta u}{dx} + \frac{\partial w}{\partial x}\frac{d\delta w}{dx} + zC\frac{\partial^2 \delta w}{\partial x^2}\right) dxdz + \frac{1}{2}\iint G_{xz}\left(\alpha + \frac{\partial w}{\partial x}\right)^2 dxdz \quad (24)$$

But,

$$\iint G_{xz}\, dxdz = G_{xz}A_{xz} = qG_{xz}A_s \quad (25)$$

Here, q is a constant (for a rectangular section, $q = 6/5$; for a circular section, $q = 37/32$), A_{xz} is the x-z plane area, A_s is the shear area and $G_{xz}A_s$ is the shear stiffness.

$$\Psi = \iint \sigma_{xx}\left(\frac{d\delta u}{dx} + \frac{\partial w}{\partial x}\frac{d\delta w}{dx} + zC\frac{\partial^2 \delta w}{\partial x^2}\right) dxdz + \frac{1}{2}qG_{xz}A_s\iint\left(\alpha + \frac{\partial w}{\partial x}\right)^2 dxdz \quad (26)$$

Integrating Eq. (26) within the depth of z leads to

$$\Psi = \int \left[N_{xx} \left(\frac{d\delta u}{dx} + \frac{\partial w}{\partial x} \frac{d\delta w}{dx} \right) + \left(M_{xx} \frac{\partial^2 \delta w}{\partial x^2} \left\{ 1 \Big/ \left(1 + \left(dw/dx \right)^2 \right)^{3/2} \right\} \right) \right] dx + \frac{1}{2} q G_{xz} A_s \int \left(\alpha + \frac{\partial w}{\partial x} \right)^2 dx \qquad (27)$$

Where

$$\int \sigma_{xx} dz = N_{xx} \; ; \qquad \int \sigma_{xx} z \, dz = M_{xx} \qquad (28)$$

N_{xx} is the axial force and M_{xx} is the bending moment in the beam. The Lagrangian function L_f is defined as

$$L_f = \sum_{r=1}^{k} \sum_{s=1}^{n} \left(T - \Psi \right)_{rs} \qquad (29)$$

The limits of the summation is from the first element $s = 1$ of each link to the last element n of the same link and $r = 1$ of each link of the mechanism to the last link k of the mechanism. Substituting the value for the total kinetic energy T from Eq. (13) and that of the strain energy density Ψ from Eq. (27), the Lagrangian can be expressed in terms of u, w, α and θ.

3. FINITE ELEMENT FORMULATION

The Rayleigh-Ritz method is used to approximate both transverse and axial deformation variables. Hermite polynomials are used to approximate the transverse displacement w, transverse shear α and beam angle θ, while the Lagrange linear interpolation functions are used to approximate the axial displacement u in order to satisfy the boundary conditions of various types of compliant mechanisms easily and to ensure interelement compatibility. It should be noted that nodes 1 and 2 are the end nodes. The axial deformation u is approximated by a shape function given by

$$u_{(x,t)} = \mathrm{g_u} U = \sum_{i=1}^{2} U_i(t) N_i(x) \qquad (30)$$

$$N_i = \left[(1 - \bar{x}), (\bar{x}) \right] \qquad (31)$$

Where N_i (i.e. $\mathrm{g_u}$) is the Lagrange interpolation function, $\bar{x}$ is the element coordinate with the origin at node 1. Let ϑ_i be the first derivative of the shape function N_i so that the approximation of Eq. (30) becomes

$$\dot{u}_{(x,t)} = \dot{g}_u U = \sum_{i=1}^{2} U_i(t) \vartheta_i(x) \qquad (32)$$

Similarly, the transverse displacement is approximated by fifth degree Hermite polynomials given by

$$w_{(x,t)} = \mathrm{g_w} \Delta = \sum_{i=1}^{6} \Delta_i(t) \phi_i(x) \qquad (33)$$

$$\Delta_1 \equiv W_1 \; ; \; \Delta_2 \equiv \Phi_2 \; ; \; \Delta_3 \equiv \Theta_3 \; ; \quad \Delta_4 \equiv W_4 \; ; \; \Delta_5 \equiv \Phi_5 ; \; \Delta_6 \equiv \Theta_6 \qquad (34)$$

$$\phi_1 = 1 - 10 \left(\frac{\bar{x}}{L} \right)^3 + 15 \left(\frac{\bar{x}}{L} \right)^4 - 6 \left(\frac{\bar{x}}{L} \right)^5 \qquad (35a)$$

$$\phi_2 = \bar{x} \left[1 - 6 \left(\frac{\bar{x}}{L} \right)^2 + 8 \left(\frac{\bar{x}}{L} \right)^3 - 3 \left(\frac{\bar{x}}{L} \right)^4 \right] \qquad (35b)$$

$$\phi_3 = \frac{\bar{x}^2}{2} \left[1 - 3 \frac{\bar{x}}{L} + 3 \left(\frac{\bar{x}}{L} \right)^2 - \left(\frac{\bar{x}}{L} \right)^3 \right] \qquad (35c)$$

$$\phi_4 = 10 \left[\left(\frac{\bar{x}}{L} \right)^3 - 15 \left(\frac{\bar{x}}{L} \right)^4 + 6 \left(\frac{\bar{x}}{L} \right)^5 \right] \qquad (35d)$$

$$\phi_5 = -\bar{x} \left[4 \left(\frac{\bar{x}}{L} \right)^2 - 7 \left(\frac{\bar{x}}{L} \right)^3 + 3 \left(\frac{\bar{x}}{L} \right)^4 \right] \qquad (35e)$$

$$\phi_6 = \frac{\bar{x}^2}{2} \left[\frac{\bar{x}}{L} - 2 \left(\frac{\bar{x}}{L} \right)^2 + \left(\frac{\bar{x}}{L} \right)^3 \right] \qquad (35f)$$

Let first and second derivatives of the displacement vector becomes

$$\dot{w}_{(x,t)} = \mathrm{g_w} \Phi = \sum_{i=2,5} \Phi_i(t) \phi_i(x) \qquad (36)$$

$$\ddot{w}_{(x,t)} = g_w \Theta = \sum_{i=3,6} \Theta_i(t)\,\phi_i(x) \tag{37}$$

For the purpose of compatibility, θ and α are also approximated by cubic polynomial

$$\theta_{(x,t)} = g_w \eta = \sum_{i=2,5} \eta_i(t)\,\phi_i(x) \tag{38a}$$

$$\dot{\theta}_{(x,t)} = g_w \varphi = \sum_{i=2,5} \varphi_i(t)\,\phi_i(x) \tag{38b}$$

$$\alpha_{(x,t)} = g_w Y = \sum_{i=1,4} Y_i(t)\,\phi_i(x) \tag{39a}$$

$$\dot{\alpha}_{(x,t)} = g_w \beta = \sum_{i=2,5} \beta_i(t)\,\phi_i(x) \tag{39b}$$

Substituting the approximations from Eqs. (30-39) into Eq. (13), the kinetic energy can now be rewritten as

$$T = \frac{1}{2}\int_{-\frac{h}{2}}^{\frac{h}{2}}\int_0^L \left[\begin{array}{l} \left(\left(b\sum_{i=2,5}\varphi_i(t)\,\phi_i(x) + \dot{x} + \sum_{i=1}^{2} U_i(t)\,\vartheta_i(x)\right)^2 + \left(a\sum_{i=2,5}\varphi_i(t)\,\phi_i(x) + \sum_{i=2,5}\Phi_i(t)\,\phi_i(x)\right)^2\right) \\ +\rho\, I_z\left(\left(\sum_{i=2,5}\beta_i(t)\,\phi_i(x)\right)^2 + \left(\begin{array}{l}\sum_{i=2,5}\varphi_i(t)\,\phi_i(x) \\ +\sum_{i=2,5}\theta_i(t)\,\phi_i(x)\end{array}\right)^2\right) \end{array}\right] dxdz \tag{40}$$

Equally, the strain energy density can be rewritten as

$$\Psi = \int_0^L \left[\begin{array}{l} \left[N_{xx}\left(\begin{array}{l}\sum_{i=j}^{2} U_j(t)\,\vartheta_j(x) \\ +\left(\sum_{j=2,5}\Phi_j(t)\,\phi_j(x)\right)^2\end{array}\right) + \left(M_{xx}\sum_{j=3,6}\Theta_j(t)\,\phi_j(x)\left\{1\Big/\left(1+\left(\sum_{j=2,5}\Phi_j(t)\,\phi_j(x)\right)^2\right)^{3/2}\right\}\right)\right] \\ +\frac{1}{2}qG_{xz}A_s\left(\begin{array}{l}\sum_{j=1,4}Y_j(t)\,\phi_j(x) \\ +\sum_{j=2,5}\Phi_j(t)\,\phi_j(x)\end{array}\right)^2 \end{array}\right] dx \tag{41}$$

$\vartheta_j(x) = \delta u(x)$ and $\phi_j(x) = \delta w(x)$. The transformation of coordinates is now introduced to change from moving coordinates system associated with the element to global coordinates. Only the nodal displacements U_i and W_i need to be transformed. The other coordinates are angles or derivative of angles which are not directional on the xz coordinate system used. The corresponding transformation is given as

$$\begin{bmatrix} U_1 \\ \Phi_1 \\ \Theta_1 \\ U_2 \\ \Phi_2 \\ \Theta_2 \end{bmatrix} = \begin{bmatrix} Cos\theta & Sin\theta & 0 & 0 & 0 & 0 \\ -Sin\theta & Cos\theta & 0 & 0 & 0 & 0 \\ 0 & 0 & Cos\theta & Sin\theta & 0 & 0 \\ 0 & 0 & -Sin\theta & Cos\theta & 0 & 0 \\ 0 & 0 & 0 & 0 & Cos\theta & Sin\theta \\ 0 & 0 & 0 & 0 & -Sin\theta & Cos\theta \end{bmatrix} \begin{bmatrix} \bar{U}_1 \\ \bar{\Phi}_1 \\ \bar{\Theta}_1 \\ \bar{U}_2 \\ \bar{\Phi}_2 \\ \bar{\Theta}_2 \end{bmatrix} \tag{42a}$$

$$\left[U_1,\ \Phi_1\ \ \Theta_1, U_2,\ \Phi_2\ \ \Theta_2\right]^T = \left[T_F\right]\left[\bar{U}_1,\ \bar{\Phi}_1\ \ \bar{\Theta}_1, \bar{U}_2,\ \bar{\Phi}_2\ \ \bar{\Theta}_2\right]^T \tag{42b}$$

T_F is the transformation matrix. $\bar{U}_1$, $\bar{\Phi}_1$ $\bar{\Theta}_1$, $\bar{U}_2$, $\bar{\Phi}_2$ $\bar{\Theta}_2$ are the nodal displacements in global coordinate. Substituting the expression from Eq. (42) into the Lagrangian equation (Eq. (29)), the equation for the global displacement vectors for the system is given as

$$L_f = \frac{1}{2}\sum_{r=1}^{k}\sum_{s=1}^{n}\left[\int_{-\frac{h}{2}}^{\frac{h}{2}}\left[\int_0^L\left[\begin{array}{l}\left(b\sum_{i=2,5}\varphi_i(t)\phi_i(x)+\dot{x}+\sum_{i=1}^{2}U_i(t)\vartheta_i(x)\right)^2+\left(a\sum_{i=2,5}\varphi_i(t)\phi_i(x)+\sum_{i=2,5}\Phi_i(t)\phi_i(x)\right)^2\\ +\rho I_z\left(\left(\sum_{i=2,5}\beta_i(t)\phi_i(x)\right)^2+\left(\sum_{i=2,5}\varphi_i(t)\phi_i(x)+\sum_{i=2,5}\theta_i(t)\phi_i(x)\right)^2\right)\end{array}\right]dxdz\right.$$
$$\left.-\int_0^L\left[\begin{array}{l}N_{xx}\left(\sum_{i=j}^{2}U_j(t)\vartheta_j(x)+\left(\sum_{j=2,5}\Phi_j(t)\phi_j(x)\right)^2\right)\\ +M_{xx}\sum_{j=3,6}\Theta_j(t)\phi_j(x)\left(1+\left(\sum_{j=2,5}\Phi_j(t)\phi_j(x)\right)^2\right)^{-3/2}\\ +\frac{1}{2}qG_{xz}A_s\left(\sum_{j=1,4}Y_j(t)\phi_j(x)+\sum_{j=2,5}\Phi_j(t)\phi_j(x)\right)^2\end{array}\right]dx\right]_{rs} \quad (43)$$

The global coordinates for the system are given by

$$q=\left[\bar{U}_1,\ \bar{\Phi}_1,\ \bar{\Theta}_1,\ \beta_1,\ \varphi_1,\ Y_1,\ \bar{U}_2,\ \bar{\Phi}_2,\ \bar{\Theta}_2,\ \beta_2,\ \varphi_2,\ Y_2\right] \quad (44)$$

Differentiating the Lagrangian with respect to the element coordinates gives the Lagrange equation of motion.

$$\frac{d}{dt}\left(\frac{\partial L_f}{\partial \dot{q}}\right)-\frac{\partial L_f}{\partial q}=0 \quad (45)$$

The operation carried out in Eq. (45) results in a system of nonlinear element differential equations. Assembling the element matrices for particular compliant mechanism being solved results in the global system of equations given as

$$[M]\{Q_{,tt}\}+[C]\{Q_{,t}\}+[K]\{Q\}=\{F\} \quad (46)$$

Where

$$[K]=[K_l]+[K_{nl}] \quad (47)$$

Q and F are the displacement and force vectors respectively. The M, C, K_l and K_{nl} matrices are all functions of time t. The C matrix results from the kinetic energy of the system. The matrix K_l is the linear portion of the stiffness matrix. The matrix K_{nl} is the nonlinear portion of the stiffness matrix. Eq. (46) give a system of nonlinear equations that will be solved iteratively for a given compliant mechanism problem. The Newton - Raphson iteration method will be employed for the iteration process.

4. NUMERICAL IMPLEMENTATION

A planar compliant four bar mechanism is analyzed and presented as shown in Fig. 4. The mechanism is constructed of polypropylene and the parameters of the mechanism are shown in Table 1. For the finite element approximation of the above formulations we used the beam elements. The entire mechanism geometry was built as adequate. The essential boundary condition was stated with the base of the mechanism clamped. Also the natural boundary condition at the tip of the mechanism is *280m*N.

Table 1. Parameters for Simulation of Results

Definition	Symbol	Value
Lengths of the mechanism links	$l_1 = l_3$ l_2	$0.7m$ $0.4m$
Young's Modulus	$E_1 = E_2 = E_3$	$1103.61MPa$
Density of material	$\rho_1 = \rho_2 = \rho_3$	$913Kg/m^3$
Poisson ratio	$v_1 = v_2 = v_3$	0.35
Breadth of the compliant links	$b_1 = b_3$ b_2	$0.00318m$ $0.00239m$
Heights of the compliant links	$h_1 = h_3$ h_2	$0.00863m$ $0.00863m$
Areas of the compliant links	$A_1 = A_3$ A_2	$27.4434\mu m^2$ $20.6257\mu m^2$
Second moments of areas of the compliant links	$I_1 = I_3$ I_2	$0.170325nm^4$ $0.128012nm$ 4

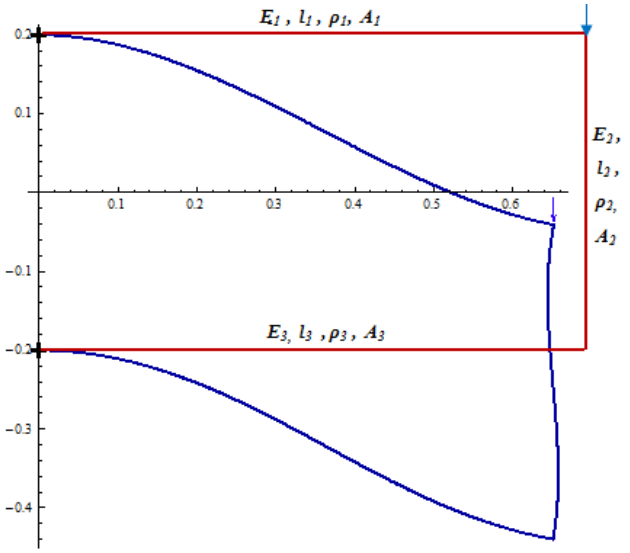

Fig. 4. Deformed and undeformed mechanism

AceGen is used for the automatic derivation of formulae needed in the numerical procedures. Symbolic derivation of the characteristic quantities (e.g. gradients, tangent operators, sensitivity vectors,…) leads to exponential behavior of derived expressions, both in time and space.

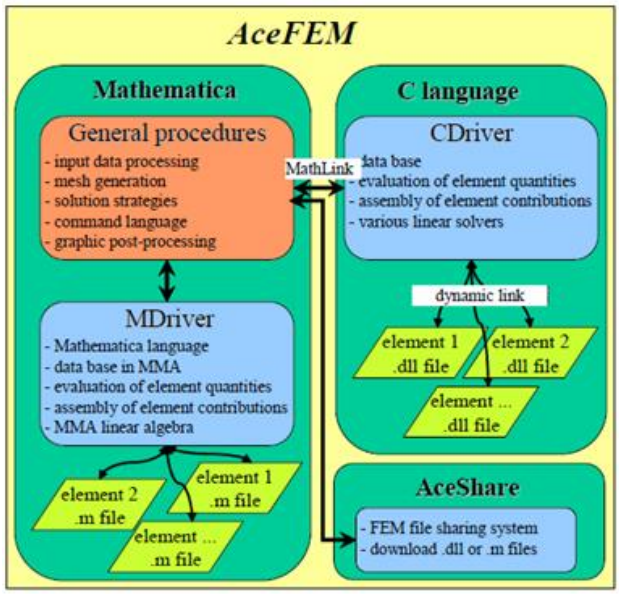

Fig. 5. System for generating a finite element code and its further analysis

AceGen offers multi-language code generation (Fortran, C, Mathematica, …) and automatic interface to general numerical environments (MathLink connection to Mathematica) and specialized finite element environments (AceFEM, FEAP, ELFEN, ABAQUS, …). Fig. 5. shows the system for generating a finite element code and its further analysis through the end compiler AceFEM.

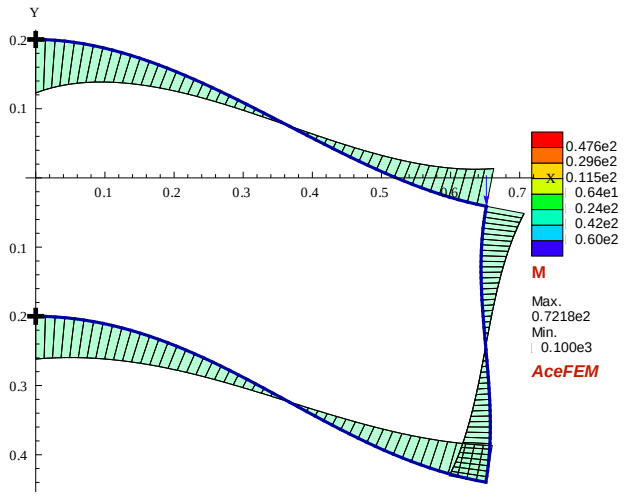

Fig. 6. Bending Moment of the deformed mechanism

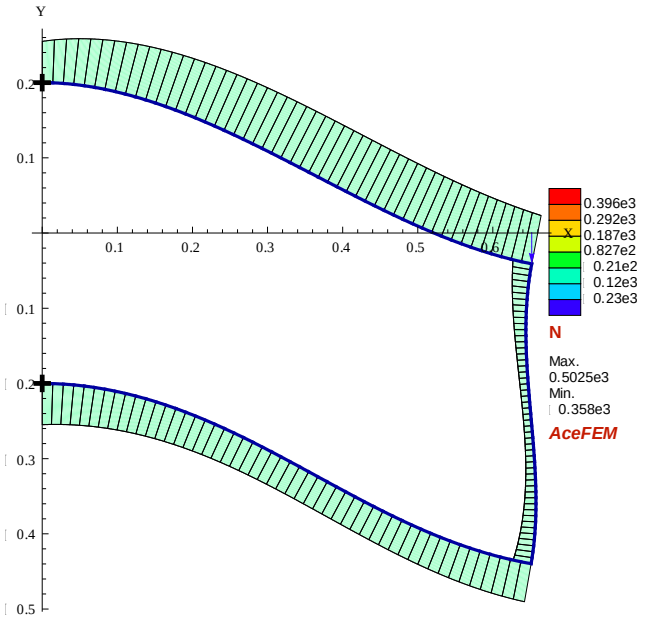

Fig. 7. Axial Force of the deformed mechanism

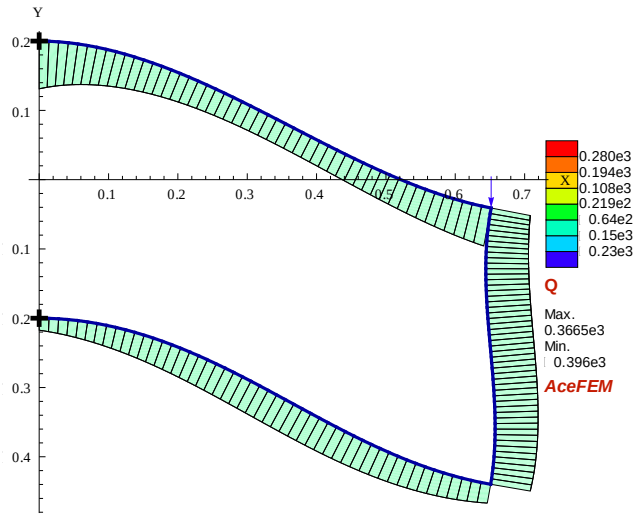

Fig. 8. Shear Force of the deformed mechanism

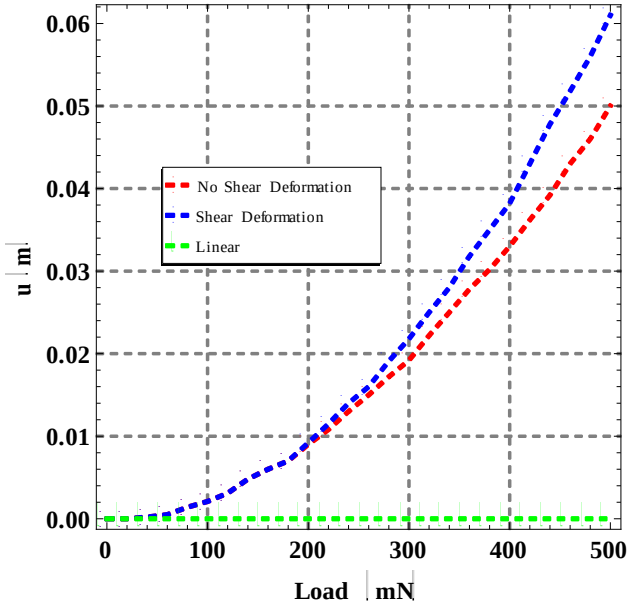

Fig. 9. Load – axial displacement u of the coupler midpoint

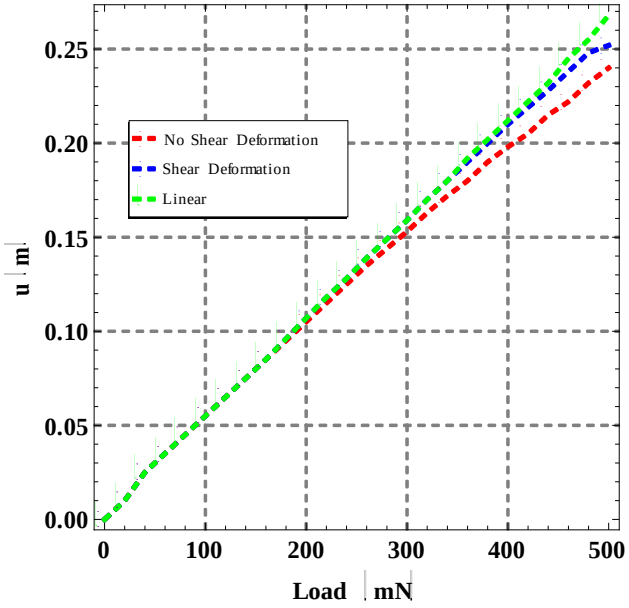

Fig. 10. Load – vertical displacement v of the coupler midpoint

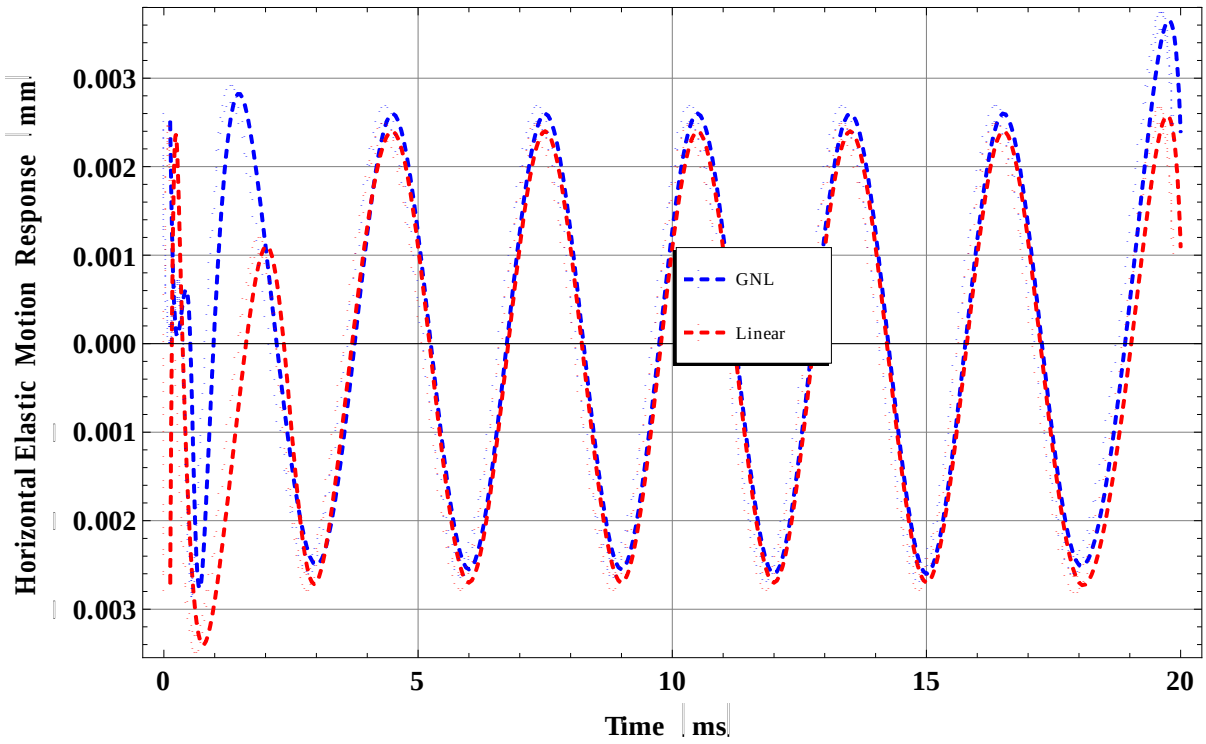

Fig. 11. Horizontal elastic motion response of the coupler midpoint

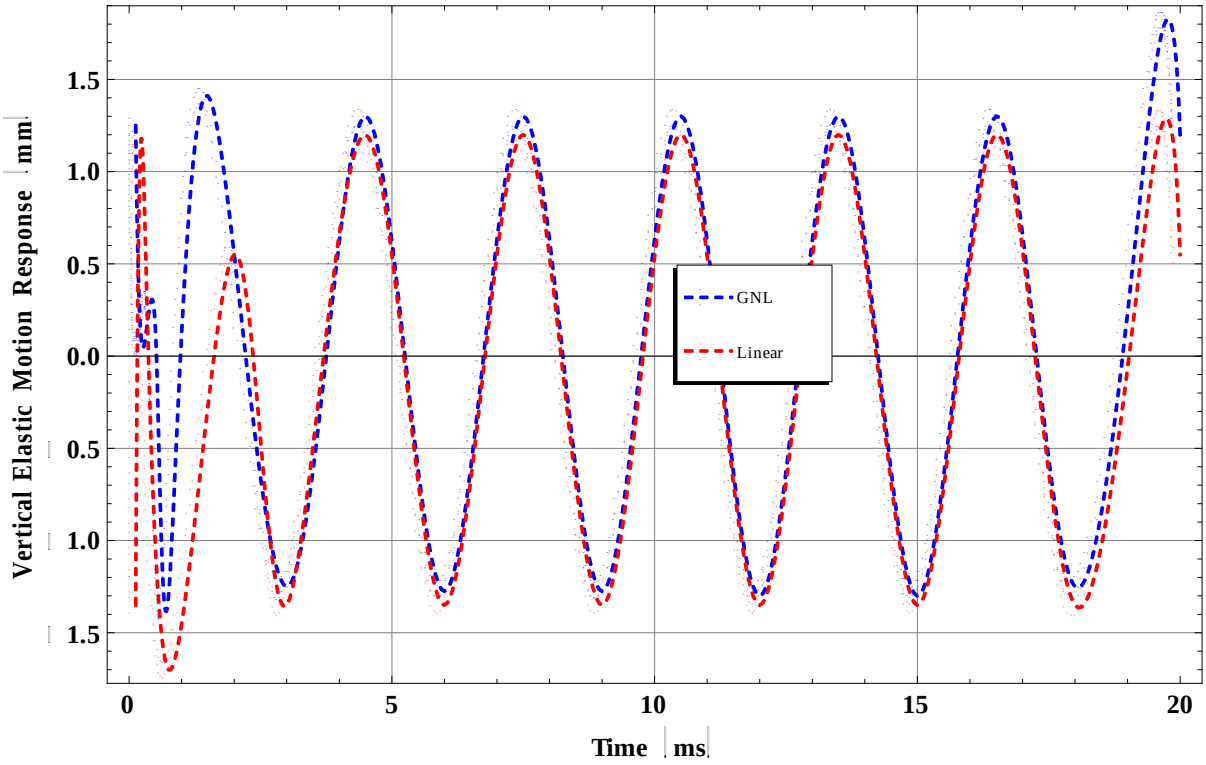

Fig. 12. Vertical elastic motion response of the coupler midpoint

5. DISCUSSION OF RESULTS

Numerical results generated for a compliant four mechanism are reported in Figs. 6. to 13. Figures 6 to 8 are the various static deformation representations of the complete mechanism. Figures 9 and 10 show the various static behavior of the coupler midpoint; in this case, the load-displacement graphs. The simulated results show a deviation from straight line graph from linear assumptions to normal curves considering the effect of geometric nonlinearity. However, there is also a deviation between the geometric nonlinear consideration when the effect of shear stress is captured and when it is not. Initially, the two nonlinear effects show the same behaviour until a point where the effect of the shear stress is much that the deviation starts becoming noticeable. The response shows an initial steady state response and later a slight increasing harmonic response. Figs. 11. and 12. are dynamic elastic response of the mechanism. Unsteady conditions are observed between 0 and 3 seconds in both cases with their produced harmonics almost overlapping between 3 and 19 seconds, after which the responses tend to separate noticeably for GNL and Linear signals. Initially, the displacement amplitude changes with each motion, stabilizes at the middle of the motion and varies towards the end of the motion cycle.

6. CONCLUSION

Figures 9 and 10 have shown that the deviation in the geometric nonlinear from the linear compliant systems analysis is great. So it is shown that the influence of the nonlinear terms in the normal strain cannot be neglected under large deflection.

It has also been established that neglecting the effect of shear stress may lead to incorrect result. The deviation between the two geometric nonlinear analyses shows a wide difference after half of the maximum input force. Therefore, the effect of shear stress must be considered when looking at the geometric nonlinear behaviour of compliant mechanisms.

In Figs. 12. and 13, linear analyses have shown to be relatively accurate in the midrange. Geometric nonlinearity effects become critically important at the end points. Failure may result from these end points despite current analysis in the midrange. This further show why compliant systems that are subjected to large deflection may still be nonlinear even with materially linear components.

REFERENCES

[1] A. G. Erdman, G. N. Sandor, Mechanisms Design: Analysis and Synthesis, Prentice Hall, Englewood Cliffs, New Delhi, 1991.

[2] L. L. Howell, Compliant Mechanisms, Wiley, New York, 2001.

[3] J. L. Herder, F.P.A. van den Berg, Statically balanced compliant mechanisms (SBCM's); an example and prospects, Proceedings ASME DETC 26th Biennial, Mechanisms and Robotics Conference, Baltimore, Maryland, paper number DETC2000/MECH-14144, 2000.

[4] T. Bele'ndez, M. Pe'ro-Polo, C. Neipp, A . Bele'ndez, Numerical and experimental analysis of large deflections of cantilever beams under a combined load, Physica scripta, 118 (2005) 61-65.

[5] K. Lee, Large defections of cantilever beams of non-linear elastic material under a combined loading, International Journal of Non-Linear Mechanics, 37, (2002) 439–443.

[6] J. Wang, J. K. Chen, S. Liao, An explicit solution of the large deformation of a cantilever beam under point load at the free tip, Journal of Computational and Applied Mathematics, 212 (2008) 320 – 330.

[7] P. B. Goncalves, D.L.B.R. Jurjio, C. Magluta, N. Roitmann, Earge deflection behavior and stability of slender bars under self weight, Structural Engineering and Mechanics, 24 (2006) 709-725.

[8] A.M.G. Dos Anjos, P. B. Goncalves, Large deflection geometrically non linear analysis of arches and beams. in: coupled instabilities in metal structures, London, Proceedings of the Coupled Instabilities in Metal Structures. London, Imperial College Press, (1996) 69-76.

[9] I. C. Ugwuoke, M. S. Abolarin, O. V. Ogwuagwu, Frequency characteristics of the compliant constant-force mechanism based on the pseudo-rigid-body model, *Assumption University Journal* of Technology (*AU J.T.*), 12 (3) (2009) 193-198.

[10] Y. Yu, L. L. Howell, Y. Yue, Dynamic modeling of compliant mechanism based on the pseudo rigid body model, journal of mech. design, 127 (2005) 760-765.

[11] S. M. Lyon, M. S. Evans, P. A. Erickson, L. L. Howell, Dynamic response of compliant mechanisms using the pseudo-rigid-body model, Proceedings of ASME Design Engineering Technical Conferences, DETC97/VIB-4177, 1997.

[12] S. M. Lyon, P. A. Erickson, L. L. Howell, Prediction of the first modal frequency of compliant mechanisms using the pseudo-rigid-body model, Journal of Mechanical Design Transactions of the ASME, 121 (2) (1999) 309-313.

[13] C. Boyle, L. L. Howell, S. P. Magleby, Dynamic modeling of compliant constant-force compression mechanisms, Mech. Mach. Theory, 38 (2003) 1469-1487.

[14] L. Saggere, S. Kota, Synthesis of Planar, Compliant four-bar mechanisms for compliant-segment motion generation, J. Mech. Des., 123 (4) (2001) 535-542.

[15] M. Rezaei, M. Tayefeh, M. Bahrami, Dynamic behavior analysis of compliant micromechanisms, Journal of Physics: Conference Series, 34 (2006) 583–588.

[16] P. Xu, Y. Jingjun, Z. Guanghua, B. Shusheng, An effective pseudo-rigid-body method for beam-based compliant mechanisms, Precision Engineering, 34 (2010) 634–639.

[17] Z. Li, and S. Kota, Dynamic analysis of compliant mechanisms, Proceedings of the ASME Design Engineering Technical Conference, 5 (2002) 43-50.

[18] W. Wang, and Y. YU, Dynamic anlysis of compliant mechanism using finite element method, Proceedings of IEEE/ASME International Conference on advanced Intelligent Mechatronics, (2008) 247-251.

[19] W. Wang, Y. Yu, Dynamic analysis of compliant mechanisms based on finite element method, Journal of Mechanical Engineering, DOI : 10.3901/JME.2010.09.079, 46 (9) 2010.

[20] X. Zhang, W. Hou, Dynamic analysis of the precision compliant mechanisms considering thermal Effect, Precision Engineering, 34 (2010) 592–606.

[21] R. Ansola, E. Veguerıa, A. Maturana, J. Canales, 3D compliant mechanisms synthesis by a finite element addition procedure, Finite Elements in Analysis and Design, 46 (2010) 760–769.

[22] B. R. Cannon, T. D. Lillian, S. P. Magleby, L. L. Howell, M. R. Linford, A compliant end-effector for microscribing, Precision Engineering, 29 (2005) 86–94.

[23] M. B. Parkinson, L. L. Howell, J. J. Cox, A parametric approach to the optimization-based design of compliant mechanism, ASME Design Engineering Technical Conference, DETC97/DAC-3763,1997.

[24] N. Tolou, J. L Herder, A semi-analytical approach to large deflections in compliant beams under point load, Delft University of Technology, Faculty of Mechanical, Maritime and Materials Engineering, Department of Biomechanical Engineering, Mekelweg 2, 2628 CD Delft, The Netherlands.

[25] A. Rubén, V. Estrella, C. Javier, J. A. Tárrago, A simple evolutionary topology optimization procedure for compliant mechanism design, Finite Elements in Analysis and Design, 44 (2007) 53 – 62.

[26] B. Zettl, W. Szyszkowski, W. J. Zhang, Accurate low DOF modeling of a planar compliant mechanism with flexure hinges: the equivalent beam methodology, Precision Engineering, 29 (2005) 237–245.

[27] J. K. Charles, K. Kota, Y. Moon, An instant center approach to the conceptual design of compliant mechanisms, International Design Engineering Technical Conference, DETC2004-57388, 2004.

[28] C. J. Shih, C. F. Lin, H. Y. Chen, An integrated design of flexure hinges and topology optimization for monolithic compliant mechanism, Society for Design and Process Science, United States of America, 2006.

[29] Z. Nia, D. Zhanga, Y. Wub, Y. Tiana, M. Huc, Analysis of parasitic motion in parallelogram compliant mechanism, Precision Engineering, 34 (2010) 133–138.

[30] N. Lobontiu, E. Garcia, Analytical model of displacement amplification and stiffness optimization for a class of flexure-based compliant mechanisms, Computers and Structures, 81 (2003) 2797–2810.

[31] J. W. Liang, F. F. Brian, Balancing energy to estimate damping in a forced oscillator with compliant contact, Journal of Sound and Vibration, 330 (2011) 2049–2061.

[32] L. Chao-Chieh, Computational Models for Design and Analysis of Compliant Mechanisms, Ph D Thesis, Georgia Institute of Technology, 2005.

[33] X. Duy, L. P. Chen, Q. H. Tian, Topology optimization design for nonlinear thermomechanical compliant actuators using meshfree method, Chinese Journal of Solid Mechanics, 29 (3) (2008) 751–758.

[34] J. Y. Joo, S. Kota, Topology synthesis of compliant mechanisms using nonlinear beam elements, Mechanics Based Design of Structures and Machines, 32(1) (2004) 17–38.

[35] Z. Jinqing, Z. Xianmin, Topology optimization of compliant mechanisms with geometrical nonlinearities using the ground structure approach, Chinese Journal of Mechanical Engineering, 24, 2011.

[36] Z. Li, X. Zhang, Topology optimization of multiple inputs and outputs compliant mechanisms with geometrically nonlinearity, Chinese Journal of Mechanical Engineering, 45(1) (2009) 180–188.

[40]

[37] A. E. Albanesi, V. D. Fachinotti, M. A. Pucheta, A. Cardona, Synthesis of compliant mechanisms for segment-motion generation tasks, Mecánica Computacional, Dynamical Systems (A), Argrentina, 26 (34) (2007) 2919 – 2930.

[38] J. Korelc, AceGEN and AceFEM manuals, 2010.

[39] J. Korelc, Symbolic Approach in Computational Mechanics and its Application to the Enchanced Strain Method, Doktorska disertacija, Darmstadt, 1996.

[i] Compliant Mechanisms
[ii] Geometric Nonlinearity
[iii] Microelectromechanical Systems
[iv] Pseudo Rigid Body Model